Journal of Magnetic Resonance 194 (2008) 46–57

Contents lists available at ScienceDirect

Journal of Magnetic Resonance

journal homepage: www.elsevier.com/locate/jmr

Hyperpolarized long-lived states in solution NMR: Three-spin case study in low field

Elena Vinogradov, Aaron K. Grant *

Department of Radiology, Beth Israel Deaconess Medical Center, Harvard Medical School, Ansin Building, Room 232, 330 Brookline Avenue, Boston, MA 02215, USA

ARTICLE INFO

Article history:
Received 2 May 2008
Available online 4 June 2008

Keywords:
Hyperpolarization
PHIP
ALTADENA
Extended lifetime
Low field
Relaxation

ABSTRACT

Recent work has shown that singlet states in two-spin systems can possess lifetimes exceeding the T_1 relaxation time, provided that the system is kept under conditions that minimize the effects of the chemical shift Hamiltonian (for instance under low magnetic field or RF irradiation). Similar observations have been made in hyperpolarized states of multi-spin systems prepared via parahydrogen-induced polarization (PHIP). However, lifetime prolongation mechanisms in multi-spin systems are still under investigation. Here we present experimental observations of a long-lived state in a three-spin system prepared by PHIP and stored at low field. The observed lifetime of the long-lived state is 144s, about twice as long as the longest T_1 measured in the system at high field. The results are analyzed using a recently proposed theory of lifetime prolongation in multi-spin systems in low field. It is shown that quantum mechanical selection rules governing intramolecular dipolar relaxation in low field account for the enhanced lifetime and spectral features of this state.

1. Introduction

Nuclear magnetic resonance is a remarkably powerful tool. However, its low intrinsic sensitivity imposes significant limitations on many of its applications. Over the years, a number of signal enhancement strategies based on hyperpolarization have been developed, including Dynamic Nuclear Polarization (DNP) [1,2] and parahydrogen-induced polarization (PHIP) [3–5]. These techniques have been applied to studies in chemistry [5] and biochemistry [6,7]. Recently, liquid-state hyperpolarized media have been applied to *in vivo* MRI [8–14]. One of the challenges of potential applications of hyperpolarized liquid media is their relatively short lifetime. Even with the use of long T_1 nuclei like ^{13}C, the lifetimes of the enhanced signals are typically a few minutes. This is a serious drawback, particularly in applications of hyperpolarization to studies of metabolic processes that require signal persistence over significantly longer time scales. Thus, prolonging hyperpolarization lifetimes may open a range of new possibilities for NMR and MRI applications.

Recently, a series of results was presented [15–17] that might help to substantially prolong the lifetime of NMR signals and can be potentially applied to hyperpolarized media. In studies of two-spin systems [15–17], it was shown that singlet states in isolated spin pairs are long-lived under suitable conditions. Such states can possess lifetimes much longer than the standard spin–lattice relaxation time T_1. The lifetime enhancements require magnetic equivalence between the two spins, which can be achieved either by keeping the samples in low field [15,17] or via application of a suitable RF pulse train [17–19]. Under these conditions, in the isolated spin pair, quantum mechanical symmetry considerations imply that the singlet state is immune to the major mechanism of relaxation in liquid-state NMR, namely intramolecular dipole–dipole interactions. Indeed, lifetimes more than an order of magnitude longer than T_1 have been observed [15,16,20]. This methodology has already been proposed for the study of slow diffusion [20] and slow dynamic processes [21]. The combination of the long-lived states with hyperpolarization may provide the means necessary to extend applications of hyperpolarized NMR and MRI to timescales that are currently inaccessible.

Long-lived states based on singlet states are of particular relevance to hyperpolarization via PHIP. This technique employs a hydrogenation reaction with parahydrogen (hydrogen gas with an excess of the spin-singlet 'para' nuclear spin state relative to the spin-triplet 'ortho' state) to produce hyperpolarized samples. Simplistically, the two hydrogen atoms that are added to the molecule during hydrogenation are in a singlet state immediately after the reaction. The singlet, however, is NMR silent, and the usual prerequisite of the successful PHIP hyperpolarized agent is that the two hydrogen atoms are magnetically inequivalent in the product compound [3]. In one version of the PHIP technique known as ALTADENA (adiabatic longitudinal transport after dissociation engenders net alignment) [22], the sample is hydrogenated outside magnet in a low field area and then adiabatically transported to high field. In this scheme the two added protons are equivalent in low field and become inequivalent at high field, where the hyperpolarization is observed. Because the sample is prepared at low field, and because long-lived states are most readily observed

* Corresponding author. Fax: +1 617 667 7917.
E-mail address: akgrant@bidmc.harvard.edu (A.K. Grant).

1090-7807/$ - see front matter © 2008 Elsevier Inc. All rights reserved.
doi:10.1016/j.jmr.2008.05.027

under low-field conditions, ALTADENA provides 'natural' conditions for observation and study of long-lived states originating from singlet states. Indeed, lifetime prolongations have been observed in generic multi-spin systems prepared using ALTADENA and stored for a period of time at low field prior to NMR measurements [23].

The mechanisms of singlet state lifetime prolongation are well understood in the case of an isolated spin pair [17]. However, in multi-spin systems the addition of one or more spins to a two-spin singlet state breaks the symmetry required for immunity from dipolar interactions. The mechanism of lifetime prolongation in multi-spin systems is still under investigation, and number of hypotheses have been proposed [24–26]. One of them, introduced in Ref. [26], shows that in the low magnetic field limit, a quantum mechanical selection rule dictates that transitions between certain pairs of states cannot be mediated by dipolar interactions. Hence, some relaxation pathways available at high field are forbidden at low field. This may lead to lifetime enhancement if *all* of the transitions from the particular state are forbidden, or if the transitions that are not expressly forbidden by the selection rule happen to be greatly suppressed. We will refer to states that have extended lifetimes due to this mechanism as long-lived Dipolar Selection Rule (DSR) states [27]. This term is introduced in order to specify a particular mechanism of lifetime prolongation and to avoid making the implication that dipolar selection rules are the only possible mechanism of lifetime prolongation.

The main purpose of the work presented here is to provide an experimental test of quantum mechanical selection rules derived earlier in Ref. [26]. We have employed 'delayed ALTADENA' experiments, similar to the scheme used in Ref. [23]. A model compound approximating an ideal three-spin system was hyperpolarized. The three-spin system is the smallest non-trivial multi-spin system that can be used for modeling relaxation dynamics in low field. An analysis of the spectral features and numerical simulations provide information about the nature of the experimentally observed long-lived state. This analysis can be also viewed as an expansion to three-spin systems of the original analysis of the ALTADENA experiment in two-spin systems [22]. The quantum mechanical selection rules governing dipolar relaxation at low field [26] are briefly re-stated here and a detailed analysis of the density matrix behavior at low field and spectral features at high field are derived. It is shown that the selection rules acting at low field [26] indeed account for the observed lifetimes and spectral features of the states observed here and in similar cases in Refs. [23,25].

2. Theory

2.1. Multi-spin system at low field

In the low magnetic field regime, where the chemical shift differences between the spins are much smaller than the scalar couplings, the motion averaged Hamiltonian contains scalar coupling terms only:

$$H_0 = \sum_{k<l} 2\pi J_{kl} \vec{I}_k \cdot \vec{I}_l \tag{1}$$

This approximation is applicable in fields where $|\delta_k - \delta_l| \ll |2\pi J_{mn}|$, i.e., where the chemical shift differences are smaller than the scalar couplings. This 'low field' regime can be achieved by either placing the sample in a weak field, or by application of suitable RF irradiation while at high field. In the following we will concentrate on the former, since this is the case of the direct relevance to the experiments discussed here. However, the theory described is extendable to the high-field case. The Hamiltonian (Eq. (1)) and the total spin, $\vec{I} = \sum_k \vec{I}_k$, can be diagonalized with the same choice of basis [26]. The energy eigenstates can be denoted by $|jm,E\rangle$, where j is the total spin angular momentum, m is the magnetic quantum number $m = -j \ldots +j$, and E is, in general, a non-angular quantum number that distinguishes between different multiplets that have the same value of j. Here it is chosen to be the energy. For instance, the three-spin system, which is of particular relevance to the following discussion, has total of 8 eigenstates: a degenerate quadruplet with $j = 3/2$ and two degenerate doublets with $j = 1/2$, each doublet characterized by an individual energy value (Fig. 1).

Intramolecular dipolar relaxation is mediated by the Hamiltonian [28]

$$H_{DD} = -\sum_{k<l} b_{kl} \left(\frac{(\vec{r}_{kl} \cdot \vec{I}_k)(\vec{r}_{kl} \cdot \vec{I}_l)}{r_{kl}^2} - \frac{1}{3} \vec{I}_k \cdot \vec{I}_l \right) \tag{2}$$

where $b_{kl} = 3\mu_0 \gamma^2 \hbar / 4\pi r_{kl}^3$ and $\vec{r}_{kl}$ is the (time-dependent) vector connecting spins k and l.

In a previous publication [26] it was shown that in the low field limit the matrix elements of the dipolar Hamiltonian (Eq. (2)) in the eigenbasis $|jm,E\rangle$ obey the following selection rule:

$$\langle j'm', E'|H_{DD}|jm,E\rangle = 0 \quad \text{if } j \neq |j'-2|, \ldots, j'+2, \tag{3}$$

which holds for all orientations of the molecule and at every instant of time. The selection rule, Eq. (3), dictates that some elements of the dipolar Hamiltonian matrix *must* vanish; however, other matrix elements may 'accidentally' be small or even vanish, depending on the specifics of the spin system.

To first-order in perturbation theory, intramolecular dipolar interactions cannot mediate transitions between states whose j values violate the selection rule in Eq. (3). This leads to a situation where equilibrium can only be achieved via higher order relaxation pathways. If, in addition, one or more of the allowed transitions along these pathways is small, it can lead to the creation of relaxation "bottlenecks" when some of the states decay significantly more slowly than others, and hence are long-lived [26]. We refer to such states as long-lived DSR states [27] in order to distinguish these states from states whose lifetimes may be prolonged by other mechanisms. The degree of enhancement will vary depending upon the geometry and scalar couplings of the system. Moreover, once a long-lived state has been identified, one can predict the NMR spectrum of this state as a function of flip angle; the experimentally acquired spectrum can then be used as an explicit test of the theoretical prediction.

2.2. Delayed ALTADENA experiments in the three-spin system

2.2.1. Low field and adiabatic transport to high field

In the three-spin system in low field the scalar coupling Hamiltonian is given by:

$$H = 2\pi(J_{12}\vec{I}_1 \cdot \vec{I}_2 + J_{13}\vec{I}_1 \cdot \vec{I}_3 + J_{23}\vec{I}_2 \cdot \vec{I}_3). \tag{4}$$

This Hamiltonian can be diagonalized using a basis set of eigenstates of the total spin angular momentum, $|jm,E\rangle$. The $j = 3/2$ states eigenvectors are given by:

$$|3/2,m\rangle = \{|\alpha\alpha\alpha\rangle, (|\alpha\alpha\beta\rangle + |\alpha\beta\alpha\rangle + |\beta\alpha\alpha\rangle)/\sqrt{3}, (|\alpha\beta\beta\rangle + |\beta\alpha\beta\rangle + |\beta\beta\alpha\rangle)/\sqrt{3}, |\beta\beta\beta\rangle\}, \tag{5}$$

and the energy of these states is:

$$E_{3/2} = \frac{\pi}{2}(J_{12} + J_{13} + J_{23}) \equiv \frac{\pi}{2}\bar{J}. \tag{6}$$

The eigenvectors for the two $j = 1/2$ doublets are given by:

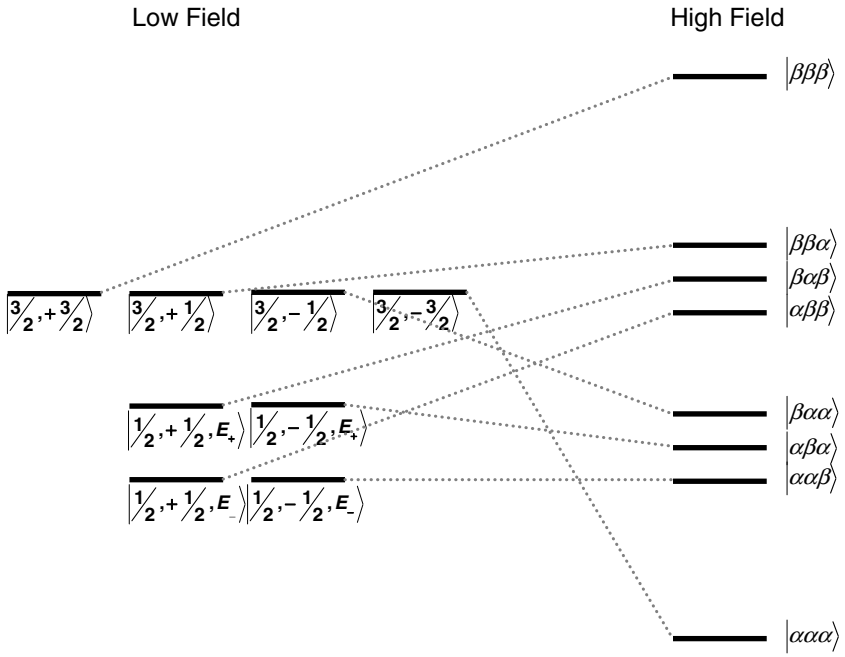

Fig. 1. Schematic energy level diagram of the three-spin system in low ($|\omega_k - \omega_l| \ll J_{mn}$) and high magnetic fields. The dotted lines indicate adiabatic transformation of the energy levels from low to high field, for the particular choice of J-couplings and chemical shift values, as discussed in the text.

$$\begin{aligned} |1/2,m,E_+\rangle &= \cos\psi|1/2,m\rangle_A + \sin\psi|1/2,m\rangle_B, \\ |1/2,m,E_-\rangle &= -\sin\psi|1/2,m\rangle_A + \cos\psi|1/2,m\rangle_B \end{aligned} \tag{7}$$

for $m = 1/2, -1/2$, and the corresponding energy eigenvalues are:

$$\begin{aligned} E_\pm &= \frac{\pi}{2}(-\bar{J} \pm 2\sqrt{J_{12}^2 + J_{13}^2 + J_{23}^2 - J_{12}J_{23} - J_{13}J_{23} - J_{12}J_{13}}) \\ &\equiv \frac{\pi}{2}(-\bar{J} \pm \Delta) \end{aligned} \tag{8}$$

In Eq. (7), ψ is a mixing angle that is a function of the scalar couplings. The expression for ψ as well as a more detailed derivation of Eqs. (5)–(8) was given in Ref. [26] and is repeated in Appendix 1 for convenience.

The low field density matrix has the general form

$$\rho^{low}(t) = \sum \rho_{jj'mm'EE'}(t)|jm,E\rangle\langle j'm',E'|. \tag{9}$$

For the case of systems prepared via PHIP, a few observations simplify the expression in Eq. (9). First, because the hydrogenation reaction is carried out over a period of a few seconds, different molecules are hydrogenated at different instants of time. Even assuming that each individual reaction is essentially instantaneous, the spread in reaction times over the population leads to an averaging of the density matrix that nulls any coherences between states of different energy. Hence the density matrix is diagonal in j and E except in the case of systems with accidental degeneracies. In addition, even very weak magnetic fields (e.g. the earth's field) will lead to further averaging that nulls coherences that are off-diagonal in m [29]. These field strengths do not give rise to significant deviations from the low-field limit described above. Finally, when parahydrogen is added to a larger molecule at low field, neither the initial molecule nor the added hydrogen nuclei carry any net angular momentum about any particular axis; consequently states with the same j and E but different m have equal populations immediately after the hydrogenation. In addition, as long as the 'low field' regime is valid, the populations of levels with the same j and E but different m values will be approximately equal at later times as well. Hence, only three population values are sufficient to describe the low-field density matrix at any time: $\rho_-(t)$, $\rho_+(t)$ and $\rho_{3/2}(t)$, corresponding to the populations of $|1/2,m,E_-\rangle$, $|1/2,m,E_+\rangle$ and $|3/2,m\rangle$, respectively. This parametrization in terms of just three populations can be validated, for the case of PHIP initial conditions, by computing the time dependence of all 8 populations as a function of time using the rate matrix derived in Ref. [26].

At low field the Boltzmann factor is extremely small, and to a good approximation the equilibrium populations are distributed equally between different energy levels. Hence, the equilibrium density matrix at low field is proportional to the identity matrix: $\rho_{eq}^{low} = \mathbf{1}/2^N$, where N is the number of spins.

In 'delayed ALTADENA' experiments [23] hydrogenation is performed at low field, followed by an evolution period at low field of varying length, τ, after which the sample is adiabatically transferred to high field where the spectrum is measured. In the adiabatic transfer the density matrix is not disturbed and the populations are preserved. The high-field energy levels depend on the specific combination of the chemical shifts (δ_i) and scalar couplings in the product compound. The high-field density matrix can be determined in terms of the low-field populations $\rho_-(\tau)$, $\rho_+(\tau)$ and $\rho_{3/2}(\tau)$ by examining the time evolution of the matrix under adiabatic transport from low field to high field. The following assumptions and observations will be used to provide a semi-quantitative analysis of the adiabatic transfer. First, we will assume that the system is weakly coupled at high field (i.e., that the scalar couplings are much smaller than the chemical shifts) and that as a result the high-field eigenstates are given by product spin states. Second, note that the m value has to be preserved throughout the transfer because the Hamiltonian commutes with I_z at all times. This is because the Hamiltonian consists of the scalar couplings in Eq. (1) together with a Zeeman term. In the case where the field is always oriented along the z axis, the Hamiltonian clearly commutes with I_z. In an actual experiment the direction of the field may undergo adiabatic changes, but provided that the changes are sufficiently slow the longitudinal magnetization is still conserved. As a result, the low-field $|3/2,-3/2\rangle$ state can only transfer into the $|\alpha\alpha\alpha\rangle$ state at high field (here we take the conven-

tion that the α state is spin-down). In general, any of the three $m = 1/2$ states in low field may transfer into any of the $m = 1/2$ high field states. The same applies to $m = -1/2$ states. The most accurate way to establish the high field populations corresponding to any given low field $m = 1/2$ (or $-1/2$) state is by performing a series of computations beginning with a low-field population in a specified state and simulating the transport of this population to high field. Here, we will assume that the eigenvalues remain distinct throughout the transfer (no energy level crossings among levels with a given m value). In this case the order of the eigenstates with a given value of m is preserved between low field and high field: the lowest energy eigenstate in low field will transfer to the lowest energy eigenstate at high field, intermediate into intermediate and the highest to highest. The resulting correspondence between low- and high-field states is indicated by the dotted lines in Fig. 1. This conclusion was verified by numerical solution of the evolution equation $i\hbar\dot{\rho}(t) = [H(t), \rho(t)]$ with a time-dependent magnetic field that begins at zero and ramps up linearly and adiabatically to 400 MHz field strength over a period of at least 10 seconds. In cases where levels with a given m value undergo crossings during adiabatic transport, numerical computations or Landau–Zener methods [30,31] can be used to determine the high-field populations. During this adiabatic transport, the system undergoes a transition from low-field relaxation dynamics to high-field relaxation dynamics. Given that the transport time is relatively short in comparison to the low-field evolution time and that the time spent at high field prior to data acquisition is also quite brief, we will assume that relaxation processes during this time do not qualitatively modify our conclusions.

Using the aforementioned arguments and assuming that $\delta_1 > \delta_2 > \delta_3$, $J_{mn} > 0$ and $|\delta_k - \delta_l| > |2\pi J_{mn}|$ the traceless part of the density matrix in the high field can be written in operator form as:

$$\rho^{high}(\tau) = (\rho_+ - \rho_-)I_z^1 I_z^3 - (\rho_+ - \rho_{3/2})I_z^1 I_z^2 - (\rho_+ - \rho_{3/2})I_z^2 I_z^3 + \frac{1}{2}(\rho_- - \rho_{3/2})(I_z^3 - I_z^1) \quad (10)$$

Where τ is the evolution time spent in low field before the beginning of the adiabatic transport period. All the populations in Eq. (10) depend on τ; the explicit dependence in Eq. (10) has been omitted for brevity. The high field matrix elements for general J_{mn} values are given in Appendix 2. Eq. (10) was derived in terms of spin operators by using the identities $|\alpha\rangle\langle\alpha| = (1/2 - I_z)$, $|\beta\rangle\langle\beta| = (1/2 + I_z)$. For instance, in the three-spin system case, $|\alpha\beta\alpha\rangle\langle\alpha\beta\alpha| = (1/2 - I_z^1)(1/2 + I_z^2)(1/2 - I_z^3)$. We emphasize again that Eq. (10) assumes that the system is weakly coupled at high field. As will be seen in the ensuing, this approximation is adequate for the qualitative description of the experimental results. However, it is by no means an exact quantitative expression valid for all chemical shifts and scalar couplings.

The observed spectrum after the application of a detection pulse on the density matrix in Eq. (10) will depend strongly on the flip angle. The qualitative spectral intensities at different frequencies as a function of the flip angle and population differences are given in Table 1.

2.2.2. Initial state

In ALTADENA experiments, the addition of parahydrogen occurs outside the magnet at low field. Because the parahydrogen carries no net spin, the density matrix of the three-spin product molecule immediately after the reaction has zero population in the $j = 3/2$ states; the initial density matrix has populations in the $j = 1/2$ states *only*. In general, these populations will deviate significantly from thermal equilibrium. Typically, the hydrogenation is carried out over a short period of time. Approximating the chemical reaction as instantaneous addition and using the quantum mechanical 'sudden' approximation to compute the initial populations, the non-trivial part of the density matrix is given by

$$\rho_\pm(0) = \frac{1}{2}\chi|\langle 1/2, m, E_\pm|s\rangle|^2, \quad \rho_{3/2} = 0 \quad (11)$$

where χ is a fraction constant in the range 0...1 and $|s\rangle$ denotes the singlet state of the added parahydrogen. The fraction constant, χ, depends on the efficiency of the chemical reaction and parahydrogen purity [4]. The enriched parahydrogen employed in our experiments was prepared at liquid nitrogen temperature and therefore contains a significant fraction of orthohydrogen. However, the presence of orthohydrogen modifies only the magnitude of the polarized spectrum, and not its shape. Hence, χ gives an overall scaling of the results and in the following it will be assumed to be equal to 1 and omitted.

The initial populations $\rho_-(0)$ and $\rho_+(0)$ will depend on the details of the hydrogenation and scalar couplings in the product compound. For the 3-spin system with spins 1, 2, and 3 labeled, as above, in order of decreasing chemical shift at high field, there are three possible hydrogenation outcomes, depending upon whether spins 1 and 2 originate from the parahydrogen, or spins 2 and 3, or spins 1 and 3. We denote these possibilities by $para_{12}$, $para_{23}$, and $para_{13}$. Using the eigenstates described above (Eqs. (5)–(8)), the initial populations for each case are given by

$$\begin{aligned}
&\rho_+(0) = \frac{1}{8}(\cos\psi + \sqrt{3}\sin\psi)^2, \quad \rho_-(0) = \frac{1}{8}(\sin\psi - \sqrt{3}\cos\psi)^2 \quad \text{for } para_{12}\\
&\rho_+(0) = \frac{1}{8}(\cos\psi - \sqrt{3}\sin\psi)^2, \quad \rho_-(0) = \frac{1}{8}(\sin\psi + \sqrt{3}\cos\psi)^2 \quad \text{for } para_{13}\\
&\rho_+(0) = \frac{1}{2}\cos^2\psi, \quad \rho_-(0) = \frac{1}{2}\sin^2\psi \quad \text{for } para_{23}
\end{aligned} \quad (12)$$

Hence, the initial population distribution will depend on the scalar couplings of the product compound through the mixing angle ψ.

It is worth noting that, immediately after hydrogenation, the intensities at the frequencies $\delta_1 \pm \frac{1}{2}(J_{12} + J_{13})$ and $\delta_3 \pm \frac{1}{2}(J_{23} + J_{13})$ will depend only on $\rho_-(0)$ because $\rho_{3/2}(0) = 0$ immediately after hydrogenation (Table 1). Likewise, the lines around δ_2 will depend only on $\rho_+(0)$.

For instance, a 90° flip at $\tau = 0$ will result in a spectrum proportional to the populations of the states $|1/2,m,E_-\rangle$ only. It is interesting to note that in this case the lines will be observed only around the spin 1 and 3 spectral positions, *irrespective* of which spins originate from parahydrogen. The overall intensity of the spectrum will change, depending on degree of the chemical yield and hyperpolarization that is achieved. An unfortunate case might occur if spins 2 and 3 originate from the parahydrogen, and the scalar couplings are such that ψ is zero or very small. In this case no intensity (or very low intensity) will be observed with a 90° detection pulse, regardless of the hyperpolarization efficiency. This marked dependence of the spectrum on the choice of flip angle is a complicating factor of PHIP measurements and was studied before in a two-spin systems [22]. These observations will be useful in interpreting the experimentally observed spectra in the light of detailed information about the density matrix at low field.

2.3. Relaxation and long-lived states

After the initial hydrogenation, the populations start to decay to their equilibrium values under the influence of various relaxation mechanisms. We shall assume that intramolecular dipolar interaction is the major relaxation mechanism for protons at low field. Using the 3 level parametrization of the full 8-by-8 relaxation ma-

Table 1
Signal intensities as a function of a flip angle (φ) and the population differences

Frequency		Intensity	Intensity (τ_0)		Intensity (τ_{long})			
			$\varphi = 90$	$\varphi = 45$	E_- long-lived		E_+ long-lived	
					$\varphi = 90$	$\varphi = 45$	$\varphi = 90$	$\varphi = 45$
δ_1	$+\frac{1}{2}(J_{12}+J_{13})$	$\sin\varphi\ \{(\rho_- - \rho_{3/2})(1+\cos\varphi)\}$	ρ_-	$1.2\rho_-$	$\rho_- - \rho_+$	$1.2\ (\rho_- - \rho_+)$	0	0
	$+\frac{1}{2}(J_{12}-J_{13})$	$\sin\varphi\{(\rho_- - \rho_+)\ (1-\cos\varphi) - (\rho_{3/2} - \rho_+)(1+\cos\varphi)\}$	ρ_-	$0.2\ \rho_- + \rho_+$	$\rho_- - \rho_+$	$0.2\ (\rho_- - \rho_+)$	0	$(\rho_+ - \rho_-)$
	$-\frac{1}{2}(J_{12}-J_{13})$	$\sin\varphi\{(\rho_- - \rho_+)\ (1+\cos\varphi) - (\rho_{3/2} - \rho_+)(1-\cos\varphi)\}$	ρ_-	$1.2\rho_- - \rho_+$	$\rho_- - \rho_+$	$1.2\ (\rho_- - \rho_+)$	0	$-(\rho_+ - \rho_-)$
	$-\frac{1}{2}(J_{12}+J_{13})$	$\sin\varphi\ \{(\rho_- - \rho_{3/2})(1-\cos\varphi)\}$	ρ_-	$0.2\rho_-$	$\rho_- - \rho_+$	$0.2\ (\rho_- - \rho_+)$	0	0
δ_2	$+\frac{1}{2}(J_{12}+J_{23})$	$2(\rho_+ - \rho_{3/2})\ \sin\varphi\cos\varphi$	0	ρ_+	0	0	0	$(\rho_+ - \rho_-)$
	$+\frac{1}{2}(J_{12}-J_{23})$	0	0	0	0	0	0	0
	$-\frac{1}{2}(J_{12}-J_{23})$	0	0	0	0	0	0	0
	$-\frac{1}{2}(J_{12}+J_{23})$	$-2(\rho_+ - \rho_{3/2})\sin\varphi\ \cos\varphi$	0	$-\rho_+$	0	0	0	$-(\rho_+ - \rho_-)$
δ_3	$+\frac{1}{2}(J_{23}+J_{13})$	$-\sin\varphi\ \{(\rho_- - \rho_{3/2})(1-\cos\varphi)\}$	$-\rho_-$	$-0.2\rho_-$	$\rho_+ - \rho_-$	$0.2(\rho_+ - \rho_-)$	0	0
	$+\frac{1}{2}(J_{23}-J_{13})$	$-\sin\varphi\{(\rho_- - \rho_+)\ (1-\cos\varphi) - (\rho_{3/2} - \rho_+)(1+\cos\varphi)\}$	$-\rho_-$	$-1.2\rho_- + \rho_+$	$\rho_+ - \rho_-$	$1.2(\rho_+ - \rho_-)$	0	$(\rho_+ - \rho_-)$
	$-\frac{1}{2}(J_{23}-J_{13})$	$-\sin\varphi\{(\rho_- - \rho_+)\ (1+\cos\varphi) - (\rho_{3/2} - \rho_+)(1-\cos\varphi)\}$	$-\rho_-$	$-0.2\rho_- - \rho_+$	$\rho_+ - \rho_-$	$0.2(\rho_+ - \rho_-)$	0	$-(\rho_+ - \rho_-)$
	$-\frac{1}{2}(J_{23}+J_{13})$	$-\sin\varphi\{(\rho_- - \rho_{3/2})\ (1+\cos\varphi)\}$	$-\rho_-$	$-1.2\rho_-$	$\rho_+ - \rho_-$	$1.2(\rho_+ - \rho_-)$	0	0

Intensities are given up to an overall factor and phase, for $J_{12} > J_{23} > J_{13}$.

trix [26], as described earlier, the evolution of populations at low field can be determined using the rate matrix:

$$\frac{d}{dt}\begin{pmatrix}\rho_+\\ \rho_-\\ \rho_{3/2}\end{pmatrix} = \frac{3\mu_0^2\gamma^4\hbar^2\tau_c}{40\pi^2 r_{12}^6}\begin{pmatrix}-10w_+ & 0 & 10w_+\\ 0 & -10w_- & 10w_-\\ 5w_+ & 5w_- & -5(w_+ + w_-)\end{pmatrix} \times \left(\begin{pmatrix}\rho_+\\ \rho_-\\ \rho_{3/2}\end{pmatrix} - \begin{pmatrix}\rho_{eq}\\ \rho_{eq}\\ \rho_{eq}\end{pmatrix}\right). \tag{13}$$

Here ρ_{eq} is the equilibrium population, $\rho_{eq} \approx 0.125$. The asymmetric form of the matrix appearing in Eq. (16) is a consequence of the different numbers of states in $j = 1/2$ multiplets and $j = 3/2$ multiplets; it is readily shown to correspond to the full 8-by-8 matrix of Ref. [26] for the special case of PHIP that is considered here. The dimensionless functions w_- and w_+ determine the rate of transitions from the two $j = 1/2$ (E_- and E_+) states to the $j = 3/2$ states and depend on the geometry of the molecule. The detailed derivation of the functions w_- and w_+, assuming the extreme narrowing regime, is given in Ref. [27]. Their explicit expressions are repeated in Appendix 3. The geometry of a 3-spin system can be described using two parameters: the ratio, λ, between $|r_{13}|$ and $|r_{12}|$ and the angle, θ, between $\vec{r}_{12}$and $\vec{r}_{13}$ (See Fig. 2, insert). The rate constants w_- and w_+ are functions of λ and θ, as well as of the mixing angle ψ. Furthermore, w_- and w_+ are connected through simple transformation $w_-(\psi) = w_+\ (\psi + \pi/2)$. As required by the selection rule in Eq. (3), the rates for direct transitions between E_- and E_+ states vanish.

Examination of the relaxation matrix Eq. (13) reveals features that can result in the creation of long-lived DSR states. First, the E_+ and E_- populations cannot equilibrate amongst themselves via direct transitions. Their equilibration process must proceed through intermediate transitions to $j = 3/2$ levels with the rates w_- and w_+. If one of the rates (w_- or w_+) happens to be small, it will create a sort of 'bottleneck' in the relaxation process, thereby stabilizing the population of one of the $j = 1/2$ states. If either of the functions w_- or w_+ happens to be exactly equal to zero the population of the one of the states becomes effectively trapped.

The solution of Eq. (13) describes the evolution of populations at low field under the influence of dipolar relaxation:

$$\rho^{low}(\tau') = \left(Q + \frac{\exp\left(-\frac{15}{2}(w_+ + w_-)\tau\prime\right)}{4S}\begin{pmatrix}3Sch + (9w_- - 7w_+)sh & -Sch - 3(w_- + w_+)sh & -2Sch + 2(-3w_- + 5w_+)sh\\ -Sch - 3(w_- + w_+)sh & 3Sch + (-7w_- + 9w_+)sh & -2Sch + 2(5w_- - 3w_+)sh\\ -Sch + (-3w_- + 5w_+)sh & -Sch + (5w_- - 3w_+)sh & 2Sch - 2(w_- + w_+)sh\end{pmatrix}\right)(\rho(0) - \rho_{eq}) + \rho_{eq}$$

with

$$S = \sqrt{9w_-^2 - 14w_-w_+ + 9w_+^2}$$
$$sh = \sinh\left(\frac{5}{2}S\tau'\right)$$
$$ch = \cosh\left(\frac{5}{2}S\tau'\right) \tag{14}$$
$$Q = \frac{1}{4}\begin{pmatrix}1 & 1 & 2\\ 1 & 1 & 2\\ 1 & 1 & 2\end{pmatrix}$$

Here $\tau' = (40\pi^2 r_{12}^6/3\mu_0^2\gamma^4\hbar^2\tau_c)t$ is a dimensionless scaled time variable. In general, the time dependence of the populations is bi-exponential. However, if either w_- or w_+ is zero (or significantly smaller than the other), one of the two exponential rates tends to zero, while the other tends to $15w_-$ or $15w_+$ depending upon whether w_+ or w_- is small. In this case the state with the vanishing (or small) decay rate becomes immune (or almost immune) to intramolecular dipolar interactions, and is consequently long-lived. The whole system will approach equilibrium slowly in these cases, with a rate dictated by the rate constant of the long-lived state. This slow decay rate can be calculated from Eq. (14) using a first-order expansion around $w_- = 0$ or $w_+ = 0$. After a long evolution period at low field this situation will result in one of the two following options for the traceless part of the density matrix operator in the high field prior to observation:

$$\rho^{high}(\tau_{long}) = e^{-\frac{40w_-\tau_{long}}{3}}\left(\frac{3\rho_-(0) - \rho_+(0)}{3}\right)\left(\frac{1}{2}(I_z^3 - I_z^1) - I_z^1 I_z^3\right)$$
for long-lived E_- state
$$\rho^{high}(\tau_{long}) = e^{-\frac{40w_+\tau_{long}}{3}}\left(\frac{3\rho_+(0) - \rho_-(0)}{3}\right)(I_z^1 I_z^3 - I_z^1 I_z^2 - I_z^2 I_z^3) \tag{15}$$
for long-lived E_+ state

Some of the populations have equilibrated between themselves in this case ($\rho_+(\tau_{long}) = \rho_{3/2}(\tau_{long})$ for long-lived E_- states and $\rho_-(\tau_{long}) = \rho_{3/2}\ (\tau_{long})$ for E_+), however they are still not equal to their equilibrium values.

Since w_- and w_+ are 90° out-of-phase in ψ, they cannot reach their minimum value simultaneously in the same molecule, and

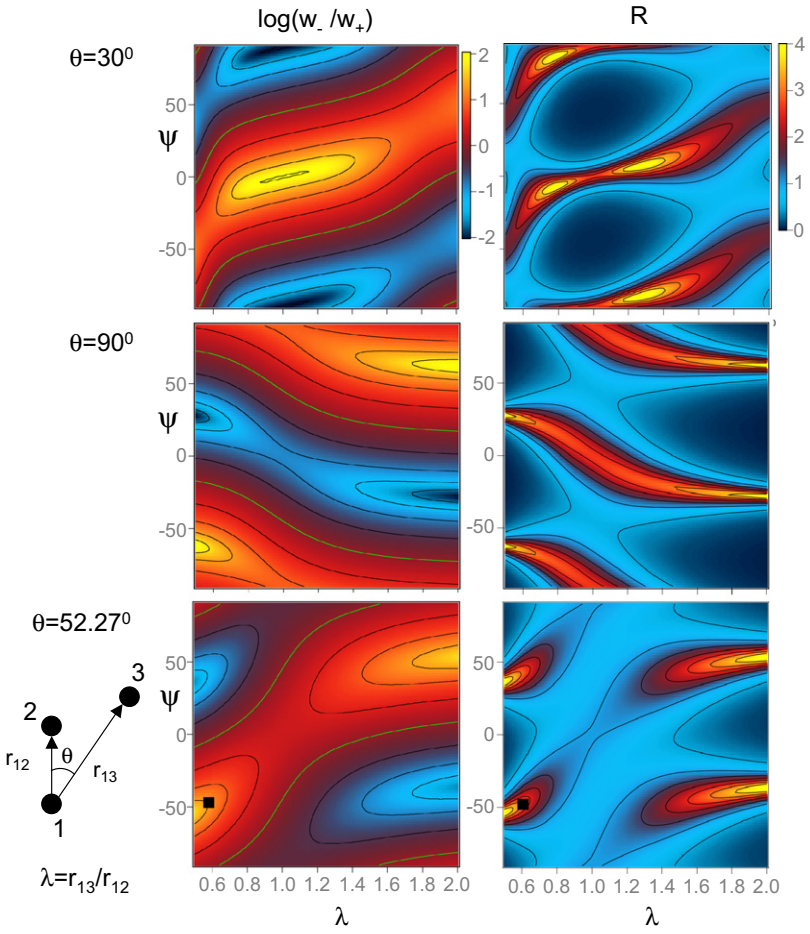

Fig. 2. Left: log (base 10) plot of the ratio, w_-/w_+, of the transition rates from the states E_- (w_-) and E_+ (w_+) which correlates with the ratio of the lifetimes of the population imbalances in the corresponding states. Yellow contour marks level 0 and the spacing of the contours is 0.5. Right: the ratio, R, of the minimum non-zero eigenvalues of the relaxation matrix in high field and low field. The spacing of the contours is 0.5. The ratios w_-/w_+ and $R$are shown as a function of ψ and λ for several values of θ:3° (top), 90° (middle), 52.42° (bottom). The black square on the bottom plots indicates estimated position of ethyl acrylate: $\theta = 52.27°$, $\lambda = 0.61$, $\psi = -47.18°$. The insert illustrates the definition of geometrical factors λ and θ.

the situation when $w_- > w_+$ or $w_+ > w_-$ may arise for a large variety of couplings and show up often in experiments. Fig. 2, left, shows the ratio w_-/w_+ for a number of geometries (parametrized by θ and λ) and scalar coupling combinations (parametrized by the mixing angle ψ). This figure can be used to predict whether one of the $j = 1/2$ states will outlive the other and by what factor for a particular molecular geometry and scalar coupling values.

Which of the two $j = 1/2$ states is long-lived can be effectively sorted out experimentally, in accordance with Eq. (15). The spectral intensities for the two cases are summarized in Table 1 and an example can be seen in Fig. 4. Notice, that in the case of a long-lived E_+ state, the density matrix is of the form $I_z^1 I_z^3 - I_z^1 I_z^2 - I_z^2 I_z^3$ and 90° detection pulse will lead to no signal at all, while a 45° flip will lead three anti-phase doublets centered on the three chemical shift values (see Table 1 and Fig. 4). These doublets are separated by the difference of the scalar couplings, $J_{12} - J_{13}$ and $J_{23} - J_{13}$, for chemical shifts of spins 1 and 3, respectively, and by the sum of the scalar couplings $J_{12} + J_{23}$ for spin 2 (Eq. (15)). This is in contrast to the anti-phase doublets obtained after application of a 45° pulse on a density matrix of the form $I_z^1 I_z^3 + I_z^1 I_z^2 + I_z^2 I_z^3$ [25], where the doublets are separated by the sum of the scalar couplings (e.g. $J_{12} + J_{13}$ for spin 1). Hence, the theory presented here and in Refs. [26,27] leads to a slightly different density matrix than that postulated in Ref. [25] (namely $I_z^1 I_z^3 - I_z^1 I_z^2 - I_z^2 I_z^3$ instead of $I_z^1 I_z^3 + I_z^1 I_z^2 + I_z^2 I_z^3$). This subtle difference predicts slight differences in the observed spectrum. The data presented here appear to support the theory of Refs. [26,27].

To estimate the possible lifetime enhancement of hyperpolarized states in low field vs. high field, the relaxation matrix, Eq. (13) can be diagonalized and the minimum non-zero eigenvalue can be compared with the minimum non-zero eigenvalue of the analogous matrix in high field. In the high field case we use the full 8-by-8 relaxation matrix corresponding to Eq. (13) for the case of a system that is weakly coupled at high field. The low-field case consists only of the sub-space relevant to the non-equilibrium states created and observed in the delayed ALTADENA process, as discussed above. The high-field relaxation matrix spans the whole 8×8 population space [26]. While other metrics can be defined, the minimum non-zero eigenvalue is relevant for the asymptotic, long time behavior of the system. Fig. 2, right, shows the ratio (R) of the minimum non-zero eigenvalues. Note that the areas where $w_- \gg w_+$ or $w_+ \gg w_-$ correspond well to the areas of substantial low-field lifetime prolongation. This is in agreement with the previous argument, that if one of the rates connecting $j = 1/2$ states becomes small it may lead to prolonged lifetimes.

3. Experimental section

3.1. Parahydrogen preparation and hydrogenation reaction

Parahydrogenation of ethyl propiolate (Scheme 1) was used in all the experiments. All the compounds are commercially available

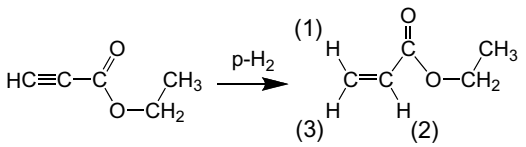

Scheme 1. Schematic of the hydrogenation reaction of ethyl propiolate with parahydrogen (p-H_2) to form ethyl acrylate. The hydrogen atoms in the product molecule that form an isolated three-spin system are marked by numbers 1, 2, and 3.

from Sigma–Aldrich (St. Louis, MO) and were used without further purification.

The parahydrogen was prepared by passing hydrogen gas through a liquid nitrogen cryostat in the presence of an ortho–para conversion catalyst (ferric hydroxide oxide (CAS 20344-49-4)).

The hydrogenation reaction was carried out in a 5 mm NMR tube equipped with septum cap. Ethyl propiolate (CAS 623-47-2) and rhodium catalyst ([1,4-bis(diphenylphosphino)butane] (1,5-cyclooctadiene)rhodium(I) tetrafluoroborate, CAS 79255-71-3) dissolved in Acetone-d_6 were placed in the NMR tube. Then, the tube was manually filled with parahydrogen, sealed, and an additional 10 mL of parahydrogen was injected through the septum cap to build extra pressure, estimated to be roughly 3 bars. The tube was manually shaken for about 5 s, and the delayed ALTADENA scheme as described in the next section, was followed. A typical sample contained about 0.5 mL of acetone-d_6, 300–400 mM concentration of ethyl propiolate, and 2 mg of the rhodium catalyst. All spectra in Figs. 3–6 were obtained with 'fresh' samples taken from a same batch of the precursor solution in order to ensure that they had the same composition. Different batches were used for Figs. 3–6.

3.2. NMR spectroscopy

All the experiments were performed on a Varian INOVA 400 MHz wide bore spectrometer using a 5 mm high-resolution probe.

Scalar couplings and chemical shift values were measured experimentally in ethyl acrylate. The experimentally measured chemical shifts were 6.28 ppm, 6.08 ppm and 5.81 ppm for protons 1, 2 and 3, respectively (the ppm scale was shifted to place δ_3 on 5.81 ppm). The experimentally measured scalar couplings were $J_{12} = 17.3$ Hz, $J_{13} = 1.4$ Hz, $J_{23} = 10.4$ Hz. These values are in the overall agreement with the values obtained from the on-line spectral database (SDBSWeb: http://riodb01.ibase.aist.go.jp/sdbs/, National Institute of Advanced Industrial Science and Technology, Japan)).

To study the dynamics of non-equilibrium states in low field conditions, delayed ALTADENA experiments [23] were performed according to the following scheme: (1) hydrogenation reaction, (2) evolution period at low field (less than 5 Gauss), (3) adiabatic transfer to high field over a period of several seconds, and (4) acquisition of an FID using 45° or 90° flip angle. The spectra were acquired after $\tau = 0$ s and 180 s using 45° or 90° flip angles. In a separate series of measurements, the spectra were acquired after 10 s, 20 s, 60 s, 120 s, 200 s, 300 s, 600 s evolution periods using a 45° flip angle.

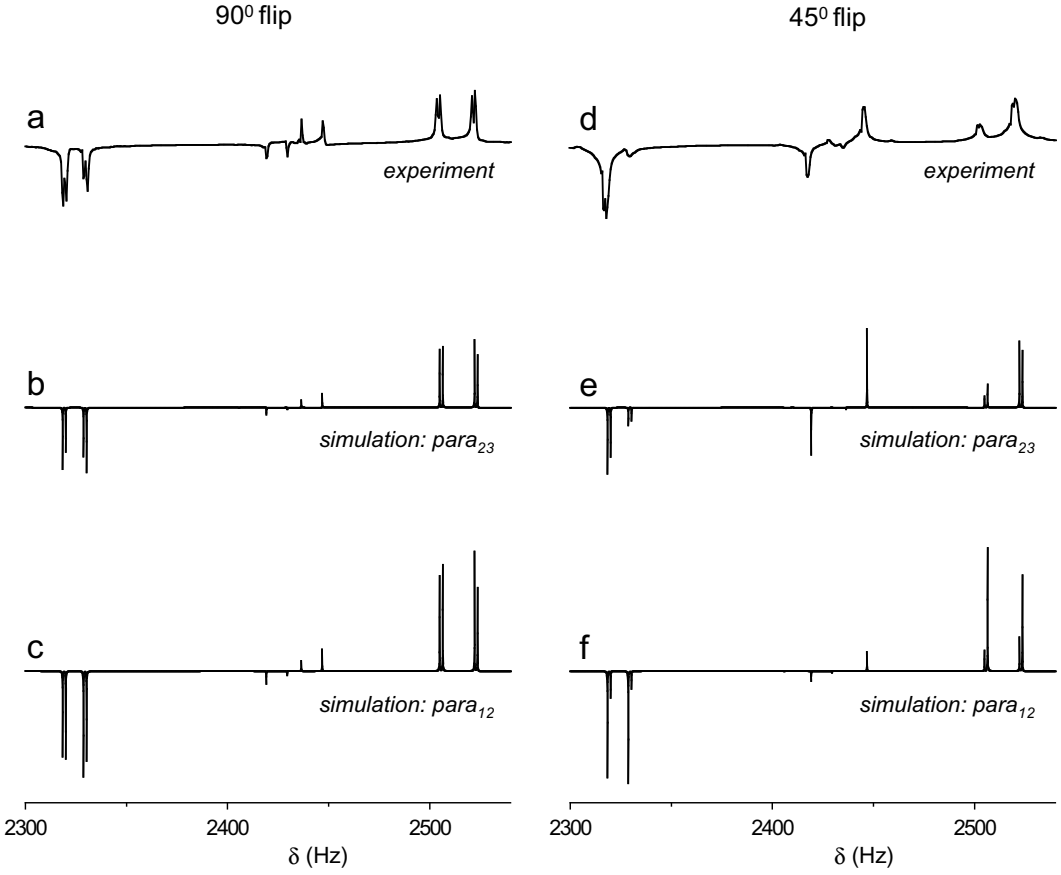

Fig. 3. Experimentally measured (a and d) and simulated (b, c, e, f) spectra acquired with 90° or 45° detection pulses (a–c and d–f, respectively) immediately after hydrogenation ($\tau = 0$) at low field. Arbitrary intensity units are used, with a common scale for the simulated spectra, and the scale of experimental spectra chosen to match that of the simulations.

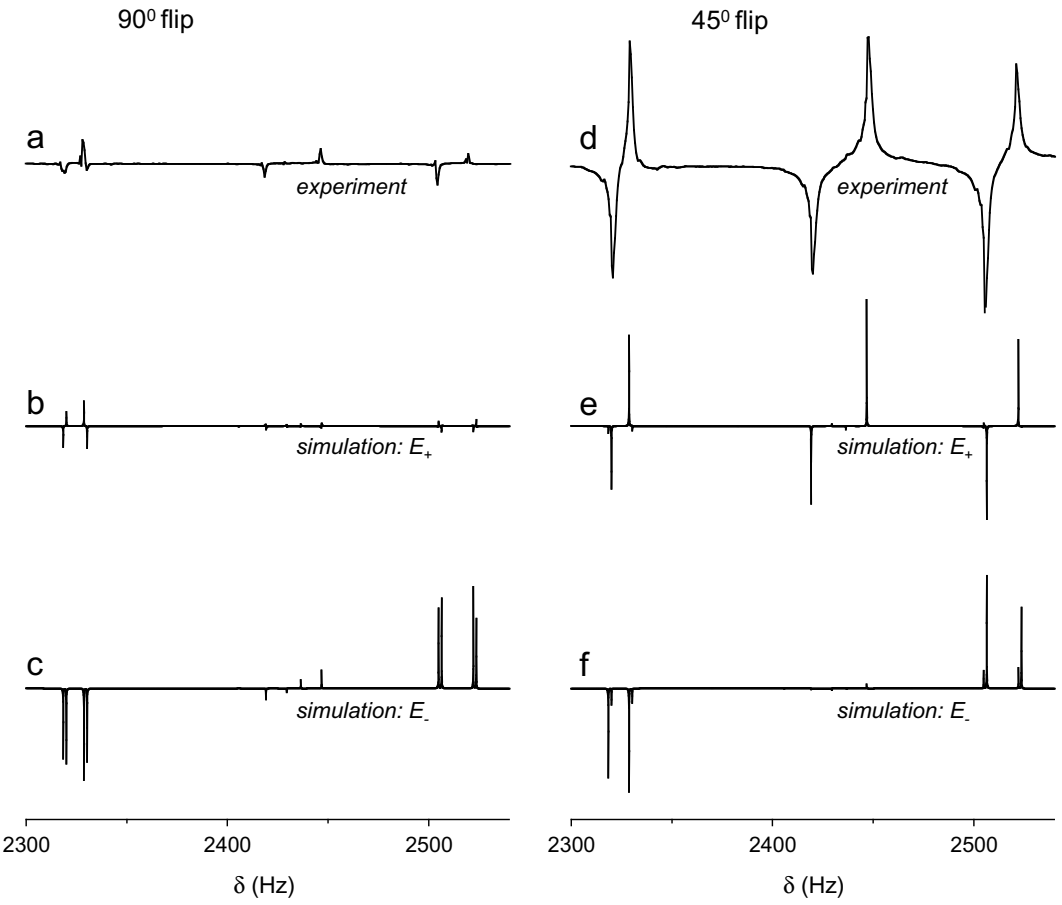

Fig. 4. Experimentally measured (a and d) and simulated (b, c, e, f) spectra, acquired with 90° or 45° detection pulse (a–c and d–f, respectively) after τ = 180 s evolution period at the low field. Arbitrary intensity units are used, with a common scale for the simulated spectra, and the scale of experimental spectra chosen to match that of the simulations.

4. Results and discussion

A schematic of the hydrogenation reaction for ethyl propiolate is shown in Scheme 1. In the product compound, ethyl acrylate, the scalar couplings of protons 1, 2, and 3 to other protons in the molecule are very weak and to a very good approximation the protons 1, 2, and 3 form an isolated three-spin system. As always, the protons were labeled in descending order of chemical shift.

Using the experimentally measured scalar coupling values in ethyl acrylate the mixing angle ψ was calculated to be -47.18 degrees. Using standard bond lengths and angles, the ratio of the vector radii lengths, λ, was calculated to be 0.61 and the bond angle between $\vec{r}_{12}$ and $\vec{r}_{13}$ is $\theta = 52.27°$. These mixing angle and geometrical parameters are used to quantify the experimental results.

Fig. 3 displays experimentally measured (a and d) and simulated (b, c, e, f) spectra acquired with a 90° or 45° detection pulse (a–c and d–f, respectively) as soon as possible after hydrogenation at low field (evolution time $\tau = 0$). Not all hydrogenation reactions have the same stereoselectivity. While it is clear that proton 2 originates from parahydrogen, it is not necessarily clear which other proton, 1 or 3, originates from parahydrogen. These two cases can be distinguished, even without numerical simulations, from analysis of the spectra obtained with different flip angles at $\tau = 0$. As described in the Theory section, addition of protons 1 and 2 corresponds to *para12* in Eq. (12), while addition of protons 2 and 3 corresponds to *para23*. The qualitative spectral intensities can be calculated by substitution of $\psi = -47.18°$ into Eq. (12) (see the discussion following the equation) and Table 1.

Qualitatively, from Eq. (12) and Table 1, the 90° pulse generates lines around chemical shifts of spins 1 and 3 only, irrespective of which of the two protons were pre-polarized. For spin 1 a quadruplet with equal intensities of 0.46 is predicted for $para_{12}$ case, while for $para_{23}$ the quadruplet lines have intensity 0.27. Same spectral features, but with the inverted intensities are expected for spin 3. Overall, this is indeed in agreement with the two simulated cases (Fig. 3, (b)-(c)). However, in the simulations and in the experiment there are also weak intensities around chemical shift of spin 2. These lines probably stem from the two sources: (i) small deviations from the weak coupling regime in the high field that was assumed here and (ii) imperfect pulse calibration (in the experimental case). The experimental set-up has additional factors that may cause deviations from the simulated spectra: the elevator speed, hardware delays and the time required for the experimenters to deliver the sample to the magnet resulted in about 8 seconds delay between the end of the evolution period and the start of the acquisition. About 4 seconds of this time is the actual adiabatic transport from low to high field. We assume that relaxation during this relatively brief period does not qualitatively modify our conclusions.

While the *cis* vs. *trans* addition can be distinguished in the simulated 90° flip spectra, it is hard to say what case ($para_{12}$ or $para_{23}$) is observed in the experiment. However, the experimental spectrum obtained with a 45° flip clearly distinguishes between the two cases: from Fig. 3 it is evident that the hydrogenation follows *cis* geometry, and that protons 2 and 3 have originated from the parahydrogen (Compare Fig. 3 (d) and (e) vs. (d) and (f)). The agree-

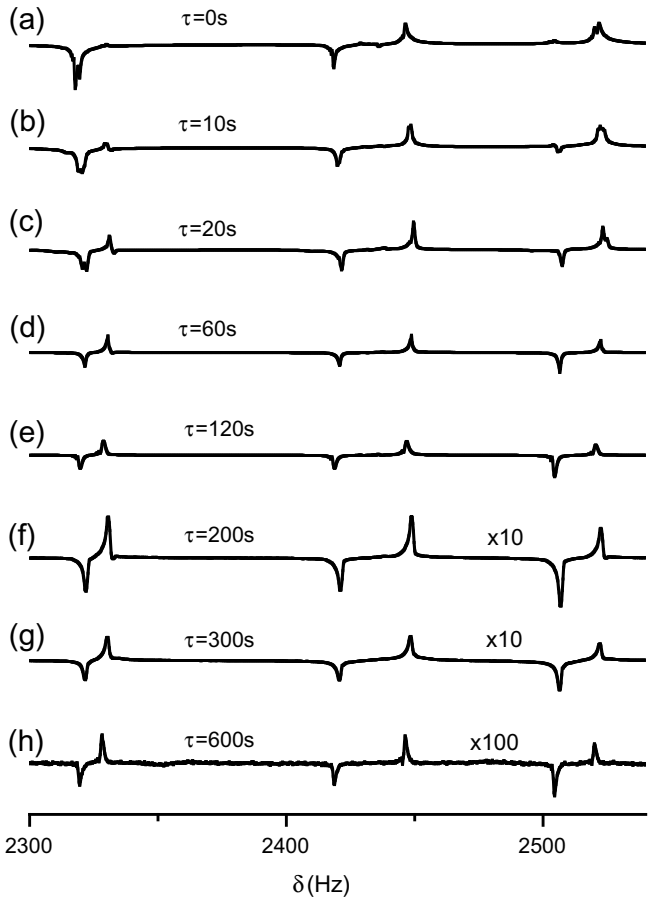

Fig. 5. Hyperpolarized spectra as a function of the evolution period at the low field: (a) 0 s, (b) 10 s, (c) 20 s, (d) 60 s, (e) 120 s, (f) 200 s, (g) 300 s, and (h) 600 s.

ment between experiment and simulations is satisfactory, and the deviations are possibly stemming from the experimental imperfections as discussed above.

Next, the evolution period was extended up to 180s. Even after this long evolution period, non-equilibrium signals were observed following a 45° pulse, as shown in Fig. 4(d). The 90° detection pulse produces essentially no signal, while 45° results in a spectrum consisting of anti-phase doublets (Fig. 4, (a) and (d)). These spectra are consistent with long-lived E_+ states, as described in Eq. (15). Using the geometrical factors and mixing angles for the ethyl acrylate, the w_-/w_+ ratio in Fig. 2 indeed predicts that the lifetime of state E_+ is about 27 times longer than that of the E_- state (the ethyl acrylate position is marked by the black square on Fig. 2, left, bottom plot). To confirm which state is long lived, simulations were performed, assuming an extra population in either the E_+ or E_- states (Fig. 4(b) and (e) or (c) and (f), respectively). These simulations confirm that the E_+ states are indeed long-lived (Compare Fig. 4 (d) and (e) vs. (d) and (f)).

Assuming that intramolecular dipolar interactions are indeed the dominant cause of spin–lattice relaxation in this system, these data lend support to the general picture of long-lived DSR states in multi-spin systems that was presented in Ref. [26]. Both the selection rule on total spin and the relaxation 'bottleneck' imposed by the small ratio of w_-/w_+ appear to be supported by the data.

To provide a more quantitative measurement of the lifetime extension, and to study the system dynamics (Eq. (15)) more closely, spectra were acquired using a 45° flip angle after evolution periods of 0s, 10s, 20s, 60s, 120s, 200s, 300s and 600s. The results of these measurements are shown in Fig. 5. All the spectral intensities are normalized by the reaction yield. Note that the line intensities dynamically change between the 0s and 60s evolution periods, and that the spectrum reaches the anti-phase shape consistent with E_+ states, as described earlier, at about 60s. Remarkably, the spectrum has still not returned to equilibrium after 600s in low field (Fig. 5, h). After this extremely long evolution period at low field, the overall intensity is low, but the shape and position of the lines still agrees with the hypothesis of long-lived E_+ states.

Next, the intensities of lines corresponding to the long-lived states were measured. One factor complicating exact quantification is that the line intensities are dependent upon both the dipolar relaxation rates as well as the rate of hydrogenation. If the

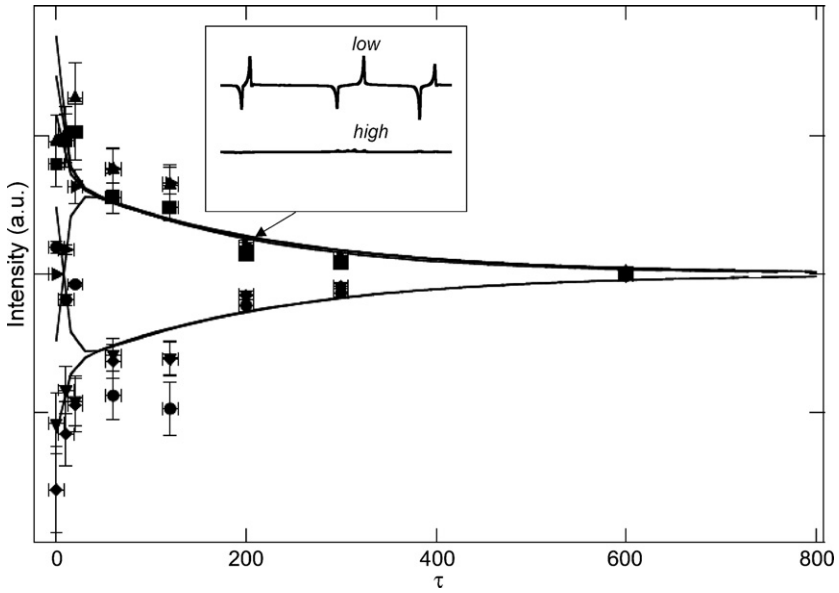

Fig. 6. The decay of the anti-phase signals as a function of the evolution period τ at low field. The symbols indicate experimental measurements of the anti-phase intensities around δ_1 (■ and ●), δ_2 (▲ and ▼) and δ_3 (► and ♦). The vertical error bars are ±20% of the signal intensity and the horizontal are ±8 s. The solid lines show calculated bi-exponential decays of the signals using Table 1 and decay lifetimes of 218 s and 9 s. The calculated intensity was vertically scaled to match the experimental data visually. The insert shows a comparison between the spectra collected after 300 s evolution period at low (top) and high (bottom) fields.

hydrogenation reaction continues for an extended period of time, then the signal intensity observed after a long delay will be significantly influenced, thereby complicating any lifetime measurements. In measuring the lifetime of the signal, we assume that the hydrogenation reaction ceases within about 13-15s after the sample is initially shaken. This is the minimum time required in our experiments between the beginning of hydrogenation and the acquisition of the spectra. To verify that 'late' hydrogenation does not significantly influence the spectra, we conducted pair of control experiments in which the reaction was quenched after a few seconds by the addition of a few microliters of DCl in D_2O (30% w/v). This addition poisons the hydrogenation catalyst and shuts off the reaction. The reaction yields and the signal enhancements are about the same in the control experiment as in all the other experiments, verifying our hypothesis that 'late' hydrogenation is not an important factor in the time evolution of the spectrum.

The intensities of six lines at the spectral positions of the long-lived spectrum are shown by symbols in Fig. 6. Accurate quantification of data acquired at short evolution periods is problematic. As was mentioned earlier, there is an inevitable delay between the adiabatic transport and data acquisition. The total time required for the adiabatic transfer, together with certain hardware delays, is about 8s. During this time the system is under the influence of relaxation processes in a varying magnetic field; we assume that relaxation during this period does not qualitatively modify our conclusions. In addition the reaction is fast, but not instantaneous. Hence, it is impossible to accurately measure lifetime constants shorter than about 8-10 s. This technical difficulty confined us to accurate measurement of the long decay constant only. Recall that: (1) the behavior is, in principle, bi-exponential and that (2) the previous results suggest that the magnitudes of the two decay constants are very different. To access the lifetime of the long-lived state the spectral intensities of the last 3 time points (at 200s, 300s and 600s) were fitted to single exponential decays and the average lifetime was found to be 144 ± 6 s. This is a significant prolongation of the lifetime, as compared with the T_1 values at high field, which were measured to be 22 ± 2 s, 67 ± 11 s, and 19 ± 4 s for spins 1, 2, and 3, respectively. Proton 2 possesses a remarkably long relaxation time at high field because of its relatively large spatial separation from the other protons. From Fig. 2 the expected enhancement of the lifetime of the low-field long-lived state compared with the standard T_1 is about 2.8. (The position of the model compound is marked by the square.) The measured ratio is about 2. The deviation might stem from a number of factors. In particular, the theoretical estimate includes only the effects of intramolecular dipolar relaxation, and furthermore includes only the effects of the three strongly coupled protons, while neglecting the effects of the other 5 protons in the molecule. In case of a long-lived state, intramolecular dipolar relaxation is strongly suppressed, and the contributions of other relaxation mechanisms become more evident. Moreover, the theoretical estimate employed the extreme narrowing limit, which may lead to overestimation of the relaxation rates in high field and hence an overestimate of the lifetime ratio. In addition, in deriving geometrical parameters we have employed standard bond lengths and angles, and not the exact structure of the ethyl acrylate, which may also contribute to the discrepancies between observed and calculated values.

To validate the model and the measurements further, the high-field dipolar relaxation rates were calculated using molecular geometry described earlier. Comparing these computed decay rates to the experimentally measured T_1 values yielded an estimate of the correlation time τ_c. Next, using the estimated correlation time and w_- and w_+ values calculated using $\theta = 52.27°$, $\lambda = 0.61$ and $\psi = -47.18°$, the lifetimes of the long- and short-lived states were estimated to be 218 s and 9 s, respectively. Given the various uncertainties described earlier, the agreement with experiment is satisfactory. In particular, the experimentally measured lifetime is expected to be shorter than the calculated one, due to additional relaxation mechanisms not included in the simple three-spin model. Using the theoretical values of the lifetimes, the time dependence of the density matrix in low field (Eq. (14)) and the spectral intensities listed in Table 1, the bi-exponential behavior of the spectral lines was calculated. The results are shown in Fig. 6 (solid lines). The agreement between the model and experiment is acceptable, particularly at the later time points. The earlier measurements are more prone to the experimental imperfections, as discussed earlier, and, hence, deviate more from the calculated curves. However, the overall behavior is bi-exponential and agrees with the model.

Finally, a second control measurement was performed at high field. The sample was adiabatically transported to high field immediately after hydrogenation and was kept there for 300 s. The resulting spectrum was compared with the analogous evolution period at low field, and both are shown in the insert in Fig. 6. The spectral intensities are much higher after evolution at low field, indicating that much faster decay occurs at high field. Closer inspection of the high-field spectrum shows that it still possesses a non-equilibrium shape, albeit of a different nature than that seen in the low-field spectra.

5. Conclusions

We have illustrated the preparation of a long-lived hyperpolarized state by means of parahydrogen-induced polarization and analyzed the results in light of recently proposed dipolar relaxation rules in low field. By storing the compound at low field following hydrogenation, the lifetime of the hyperpolarized signal can be significantly extended relative to the high-field T_1 relaxation time.

These data qualitatively support the picture of long-lived states in multi-spin systems that was presented in Ref. [26]. The selection rule for intramolecular dipolar relaxation in combination with 'bottlenecks' in the relaxation process may give rise to long-lived DSR states. We have shown that this model predicts the existence of a long-lived $j = 1/2$ DSR state whose spectrum matches the spectrum that is observed at late times. The state was identified experimentally and the measured lifetime was 144 ± 6 s, about 2 times longer the longest T_1observed in the system in the high field. The exact lifetime of this state depends upon a number of parameters, including the correlation time for the molecular tumbling and the relaxation rate due to additional intra- and extra-molecular relaxation mechanisms. However, in spite of these uncertainties, the main expectations of this model appear to be borne out by the data.

The analysis presented here may help to develop a protocol for the extension of signal lifetimes for *in vitro* and *in vivo* studies using liquid hyperpolarized media. The spectral lineshapes depend on the molecular structure and the experimental details of the PHIP experiment. Hence, in the future, imaging sequences for these agents can be tailored for better utilization of the hyperpolarized signals. In addition, certain spectroscopic features of the experiments could assist in the studies of hydrogenation reaction mechanisms.

Acknowledgments

We thank Prof. R.E. Lenkinski (Beth Israel Deaconess Medical Center, Boston, MA) for stimulating discussions and suggestions during the work. We are grateful to Prof. J.A. Balschi (Brigham

and Women's Hospital, Boston, MA) for use of the NMR equipment and help with the experiments.

Appendix 1

The low field Hamiltonian Eq. (4) can be diagonalized using a basis set of eigenstates of the total spin angular momentum, $|jm,E\rangle$. The $j = 3/2$ eigenstates correspond to the highest angular momentum value and can readily be found:

$$|3/2,m\rangle = \{|\alpha\alpha\alpha\rangle, (|\alpha\alpha\beta\rangle + |\alpha\beta\alpha\rangle + |\beta\alpha\alpha\rangle)/\sqrt{3}, (|\alpha\beta\beta\rangle + |\beta\alpha\beta\rangle + |\beta\beta\alpha\rangle)/\sqrt{3}, |\beta\beta\beta\rangle\}.$$

These states are degenerate eigenstates of the Hamiltonian with energy $E_{3/2} = \frac{\pi}{2}(J_{12}+J_{13}+J_{23}) \equiv \frac{\pi}{2}\bar{J}$.

The three-spin system also possesses two $j = 1/2$ doublets. To define these, we start with a set $\{|1/2,m\rangle_A, |1/2,m\rangle_B\}$ which are eigenstates of the total angular momentum, but not the Hamiltonian, Eq. (4). The choice of the set $\{|1/2,m\rangle_A, |1/2,m\rangle_B\}$ is not unique. We choose the 'A' state to have spins 2 and 3 to be in a singlet state, and the 'B' state to be the orthogonal $j = 1/2$ state, which is thus defined up to an overall phase:

$$|1/2,m\rangle_A = \{(|\alpha\alpha\beta\rangle - |\alpha\beta\alpha\rangle)/\sqrt{2}, (|\beta\alpha\beta\rangle - |\beta\beta\alpha\rangle)/\sqrt{2}\}$$
$$|1/2,m\rangle_B = \{(2|\beta\alpha\alpha\rangle - |\alpha\alpha\beta\rangle - |\alpha\beta\alpha\rangle)/\sqrt{6}, -(2|\alpha\beta\beta\rangle - |\beta\alpha\beta\rangle - |\beta\beta\alpha\rangle)/\sqrt{6}\}$$

The $j = 1/2$ energy eigenstates of Hamiltonian in Eq. (4) can be expressed in terms of these states using a single mixing angle ψ:

$$|1/2,m,E_+\rangle = \cos\psi|1/2,m\rangle_A + \sin\psi|1/2,m\rangle_B,$$
$$|1/2,m,E_-\rangle = -\sin\psi|1/2,m\rangle_A + \cos\psi|1/2,m\rangle_B$$

for $m = 1/2, -1/2$, with the eigenvalues

$$E_\pm = \frac{\pi}{2}\left(-\bar{J} \pm 2\sqrt{J_{12}^2+J_{13}^2+J_{23}^2-J_{12}J_{23}-J_{13}J_{23}-J_{12}J_{13}}\right) \equiv \frac{\pi}{2}(-\bar{J} \pm \Delta).$$

The mixing angle ψ is given by

$$\tan\psi = \frac{-J_{12}-J_{13}+2J_{23}+\Delta}{\sqrt{3}(-J_{12}+J_{13})}.$$

Appendix 2

In this appendix the transformation of the low field density matrix elements into the high field elements in the adiabatic transfer is derived for a three-spin system.

The m values are conserved in the transfer; hence we shall distinguish four groups of low field populations based on the m values and ratios of the eigenvalues.

(i) the populations of the $|3/2,\pm 3/2\rangle$ states, $\rho^{low}_{3/2,\pm3/2} \equiv d(|3/2,3/2\rangle\langle 3/2,3/2| + |3/2,-3/2\rangle\langle 3/2,-3/2|)$

(ii) the populations of the lowest energy eigenstates with $m = \pm 1/2$, $\rho^{low}_{\min} \equiv a(|j,1/2,E_{\min}\rangle\langle j,1/2,E_{\min}| + |j,-1/2,E_{\min}\rangle\langle j,-1/2,E_{\min}|)$

(iii) the populations of the intermediate energy eigenstates with $m = \pm 1/2$, $\rho^{low}_{\rm int} \equiv b(|j,1/2,E_{\rm int}\rangle\langle j,1/2,E_{\rm int}| + |j,-1/2,E_{\rm int}\rangle\langle j,-1/2,E_{\rm int}|)$

(iv) the populations of the higest energy eigenstates with $m = \pm 1/2$, $\rho^{low}_{\max} \equiv c(|j,1/2,E_{\max}\rangle\langle j,1/2,E_{\max}| + |j,-1/2,E_{\max}\rangle\langle j,-1/2,E_{\max}|)$

Note that while for the energies of the $j = 1/2$ states the relation $E_+ > E_-$ is always true, the energy of the $j = 3/2$ states can be lower or higher than the eigenvalues of the $j = 1/2$ states, depending on the signs of the scalar couplings. Hence, a, b, c can correspond to any of the $m = \pm 1/2$ states.

The m value has to be preserved throughout the transfer. We assume that during the adiabatic transfer the eigenvalues remain distinct throughout the whole transition period. Hence, the order of the eigenstates is preserved. Assuming that j-couplings are much smaller than the chemical shift differences in high field, the high field eigenstates are given by the product states. Without the loss of generality we shall assume that $\delta_1 > \delta_2 > \delta_3$. The identities $|\alpha\rangle\langle\alpha| = (1/2 - I_z)$ and $|\beta\rangle\langle\beta| = (1/2 + I_z)$ are used to derived the high field density matrix in terms of spin operators. Using the above notation we obtain the following traceless parts of the density matrix in the high field:

(i) $\rho^{low}_{3/2,\pm3/2} \to d\left(I_z^1 I_z^2 + I_z^1 I_z^3 + I_z^2 I_z^3\right)$

(ii) $\rho^{low}_{\min} \to a\left(-I_z^1 I_z^2 + \frac{1}{2}(I_z^3 - I_z^1)\right)$

(iii) $\rho^{low}_{\rm int} \to b\left(-I_z^1 I_z^2 + I_z^1 I_z^3 - I_z^2 I_z^3\right)$

(iv) $\rho^{low}_{\max} \to c\left(-I_z^1 I_z^3 - \frac{1}{2}(I_z^3 - I_z^1)\right)$

For example, Eq. (10) in the text can be obtained for the case when $|j,1/2,E_{\min}\rangle = |1/2,1/2,E_-\rangle$, $|j,1/2,\ E_{\rm int}\rangle = |1/2,1/2,E_+\rangle$ and $|j,1/2,\ E_{\max}\rangle = |3/2,1/2\rangle$ (similar for $m = -1/2$). In this case $d = c = \rho_{3/2}$, $a = \rho_-$ and $b = \rho_+$.

Other cases with different order between the eigenstates in the low field can be treated similarly, making suitable substitutions for a, b, c, d.

Appendix 3

The dimensionless functions w_- and w_+ referred to in the text are given by:

$$w_+ \equiv \frac{1}{10}[A(\lambda,\theta) + B(\lambda,\theta)\cos 2\psi + C(\lambda,\theta)\sin 2\psi]$$

with

$$A(\lambda,\theta) = \frac{5}{96}\left\{4 + \frac{4}{Q^3} - \frac{4}{Q^{5/2}} - \frac{\lambda^3+4\lambda^5+\lambda^8+Q^{5/2}[\lambda^3-4]}{Q^{5/2}\lambda^6} + \frac{8\lambda[\lambda^3+1]\cos\theta - 3[1+Q^{5/2}+\lambda^5]\cos 2\theta}{Q^{5/2}\lambda^3}\right\}$$

$$B(\lambda,\theta) = \frac{5}{96Q^3\lambda^6}\left\{2Q^3[1-\lambda^3+\lambda^6] - 4\lambda^6 + Q^{1/2}\lambda^3\left[1+4\lambda^2+4\lambda^3+\lambda^5 - 8\lambda(1+\lambda^3)\cos\theta + 3(1-2Q^{5/2}+\lambda^5)\cos 2\theta\right]\right\}$$

$$C(\lambda,\theta) = -\frac{5}{16\sqrt{3}}\left\{1 - \frac{1}{\lambda^6} + \frac{1+4\lambda^2-4\lambda^3-\lambda^5+8\lambda[\lambda^3-1]\cos\theta - 3[\lambda^5-1]\cos 2\theta}{2Q^{5/2}\lambda^3}\right\},$$

where $Q = 1 + \lambda^2 - 2\lambda\cos\theta$.

In addition, w_- and w_+ are connected through the transformation:

$$w_-(\lambda,\theta,\psi) = w_+\left(\lambda,\theta,\psi - \frac{\pi}{2}\right).$$

References

[1] A.W. Overhauser, Polarization of nuclei in metals, Phys. Rev. 92 (2) (1953) 411–415.
[2] A. Abragam, M. Goldman, Principles of dynamic nucelar polarization, Rep. Prog. Phys. 41 (1978) 395.
[3] C.R. Bowers, D.P. Weitekamp, Transformation of symmetrization order to nuclear-spin magnetization by chemical reaction and nuclear magnetic resonance, Phys. Rev. Lett. 24 (1986) 2645–2648.
[4] C.R. Bowers, D.P. Weitekamp, Parahydrogen and synthesis allow dramatically enhanced nuclear alignment, J. Am. Chem. Soc. 109 (1987) 5541–5542.
[5] J. Natterer, J. Bargon, Parahydrogen induced polarization, Prog. Nucl. Magn. Reson. Spectrosc. 31 (1997) 215–293.
[6] D.A. Hall, D.C. Maus, G.J. Gerfen, S.J. Inati, L.R. Becerra, F.W. Dahlquist, R.G. Griffin, Polarization-enhanced NMR spectroscopy of biomolecules in frozen solution, Science 276 (1997) 930–932.
[7] M. Rosay, J.C. Lansing, K. Haddad, W.W. Bachovchin, J. Herzfeld, R.J. Temkin, R.G. Griffin, High_frequency dynamic nuclear polarization in MAS spectra of membrane and soluble proteins, J. Am. Chem. Soc. 125 (45) (2003) 13626–13627.
[8] K. Golman, J.H. Ardenkjaer-Larsen, J.S. Petersson, S. Mansson, I. Leunbach, Molecular imaging with endogenous substances, Proc. Natl. Acad. Sci. USA 100 (2003) 10435–10439.
[9] J.H. Ardenkjaer-Larsen, B. Fridlund, A. Gram, G. Hansson, L. Hansson, M.H. Lerche, R. Servin, M. Thaning, K. Golman, Increase in signal-to-noise ration of >10000 times in liquid-state NMR, Proc. Natl. Acad. Sci. USA 100 (18) (2003) 10158–10163.
[10] K. Golman, J.H. Ardenkjaer-Larsen, J.S. Petersson, S. Mansson, L. Ib, Molecular imaging with endogenous substances, Proc. Natl. Acad. Sci. USA 100 (2003) 10435–10439.
[11] K. Golman, R. in't Zandt, M. Thaning, Real-time metabolic imaging, Proc. Natl. Acad. Sci. USA 103 (2006) 11270–11275.
[12] A.P. Chen, M.J. Albers, C.H. Cunningham, S.J. Kohler, Y.-F. Yen, R. Hurd, J. Tropp, R. Bok, J.M. Pauly, S. Nelson, J. Kurhanewicz, D.B. Vigneron, Hyperpolarized C13 spectroscopic imaging of the TRAMP mouse at 3T-initial experience, Magn. Reson. Med. 58 (2007) 1099–1106.
[13] S.J. Kohler, Y. Yen, J. Wolber, A.P. Chen, M.J. Albers, R. Bok, V. Zhang, J. Tropp, S. Nelson, D.B. Vigneron, J. Kurhanewicz, R.E. Hurd, In vivo C13 metabolic imaging at 3T with hyperpolarized C13-1-pyruvate, Magn. Reson. Med. 58 (2007) 65–69.
[14] M. Goldman, H. Johannesson, O. Axelsson, M. Karlsson, Hyperpolarization of 13C through order transfer from parahydrogen: a new contrast agent for MRI, Magn. Reson. Imag. 23 (2005) 153–157.
[15] M. Carravetta, O.G. Johannesson, M.H. Levitt, Beyond the T1 limit: singlet nuclear spin states in low magnetic fields, Phys. Rev. Lett. 92 (15) (2004) 153003.
[16] M. Carravetta, M.H. Levitt, Long-lived nuclear spin states in high-field solution NMR, J. Am. Chem. Soc. 126 (2004) 6228–6229.
[17] M.H. Levitt, M. Carravetta, Theory of long-lived spin states in solution nuclear magnetic resonance. I. Singlet states in low magnetic fields, J. Chem. Phys. 122 (2005) 214505–214514.
[18] K. Gopalakrishnan, G. Bodenhausen, Lifetimes of the singlet-states under coherent off-resonance irradiation in NMR spectroscopy, J. Magn. Reson. 182 (2006) 254–259.
[19] R. Sarkar, P. Ahuja, D. Moskau, P.R. Vasos, G. Bodenhausen, Extending the scope of singlet-state spectroscopy, Chem. Phys. Chem. 8 (2007) 2652–2656.
[20] S. Cavadini, J. Dittmer, S. Antonijevic, G. Bodenhausen, Slow diffusion by singlet state NMR spectroscopy, J. Am. Chem. Soc. 127 (2005) 15744–15748.
[21] R. Sarkar, P.R. Vasos, G. Bodenhausen, Singlet-state exchange NMR spectroscopy for the study of very slow dynamic processes, J. Am. Chem. Soc. 129 (2) (2007) 328–334.
[22] M.G. Pravica, D.P. Weitekamp, Net NMR alignment by adiabatic transport of parahydrogen addition products to high magnetic field, Chem. Phys. Lett. 145 (4) (1988) 255–258.
[23] T. Jonischkeit, U. Bommerich, J. Stadler, K. Woelk, H.G. Niessen, J. Bargon, Generating long-lasting H-1 and C-13 hyperpolarization in small molecules with parahydrogen-induced polarization, J. Chem. Phys. 124 (20) (2006) 201109.
[24] G. Pileio, M.H. Levitt, J-stabilization of singlet states in the solution NMR of multiple-spin systems, J. Magn. Reson. 187 (2007) 141–145.
[25] D. Canet, S. Bouguet-Bonnet, C. Aroulanda, F. Reineri, About long-lived nuclear spin states involved in para-hydrogenated molecules, J. Am. Chem. Soc. 129 (5) (2007) 1445–1449.
[26] E. Vinogradov, A.K. Grant, Long-lived states in solution NMR: selection rules for intramolecular dipolar relaxation in low magnetic fields, J. Magn. Reson. 188 (2007) 176–182.
[27] A. Grant, E. Vinogradov, Long-lived states in solution NMR: theoretical examples in three- and four-spin systems, J. Magn. Reson., in press, doi:10.1016/j.jme.2008.04.030.
[28] A. Abragam, in: W. Marshall, D. Wilkinson (Eds.), The Principles of Nuclear Magnetism, Clarendon Press, Oxford, 1961.
[29] H. Johannesson, O. Axelsson, M. Karlsson, Transfer of para-hydrogen spin order into polarization by diabatic field cycling, CR Phys. 5 (2004) 315–324.
[30] L.D. Landau, On the theory of transfer of energy at collisions II, Phys. Z Sowjetunion 2 (1932) 46.
[31] C. Zener, Non-adiabatic crossing of energy levels, Proc. R. Soc. Lond. A 137 (833) (1932) 696–702.